Biochemical Pharmacology 78 (2009) 420–429

Contents lists available at ScienceDirect

Biochemical Pharmacology

journal homepage: www.elsevier.com/locate/biochempharm

Crystal structures of human group-VIIA phospholipase A2 inhibited by organophosphorus nerve agents exhibit non-aged complexes☆,☆☆

Uttamkumar Samanta [a], Stephen D. Kirby [a,b], Prabhavathi Srinivasan [a], Douglas M. Cerasoli [b], Brian J. Bahnson [a,*]

[a] Department of Chemistry & Biochemistry, University of Delaware, Newark, DE 19716, USA
[b] U.S. Army Medical Research Institute of Chemical Defense, Aberdeen Proving Ground, MD 21010, USA

ARTICLE INFO

Article history:
Received 5 February 2009
Accepted 16 April 2009

Keywords:
Phospholipase A2
Lp-PLA2
PAF-AH
Organophosphate
Nerve agent

ABSTRACT

The enzyme group-VIIA phospholipase A2 (gVIIA-PLA2) is bound to lipoproteins in human blood and hydrolyzes the ester bond at the *sn-2* position of phospholipid substrates with a short *sn-2* chain. The enzyme belongs to a serine hydrolase superfamily of enzymes, which react with organophosphorus (OP) nerve agents. OPs ultimately exert their toxicity by inhibiting human acetycholinesterase at nerve synapses, but may additionally have detrimental effects through inhibition of other serine hydrolases. We have solved the crystal structures of gVIIA-PLA2 following inhibition with the OPs diisopropylfluorophosphate, sarin, soman and tabun. The sarin and soman complexes displayed a racemic mix of P_R and P_S stereoisomers at the P-chiral center. The tabun complex displayed only the P_R stereoisomer in the crystal. In all cases, the crystal structures contained intact OP adducts that had not aged. Aging refers to a secondary process OP complexes can go through, which dealkylates the nerve agent adduct and results in a form that is highly resistant to either spontaneous or oxime-mediated reactivation. Non-aged OP complexes of the enzyme were corroborated by trypsin digest and matrix-assisted laser desorption ionization mass spectrometry of OP-enzyme complexes. The lack of stereoselectivity of sarin reaction was confirmed by gas chromatography/mass spectrometry using a chiral column to separate and quantitate the unbound stereoisomers of sarin following incubation with enzyme. The structural details and characterization of nascent reactivity of several toxic nerve agents is discussed with a long-term goal of developing gVIIA-PLA2 as a catalytic bioscavenger of OP nerve agents.

1. Introduction

The enzyme group-VIIA phospholipase A2 (gVIIA-PLA2, *EC 3.1.1.47*) hydrolyzes the ester bond at the *sn-2* position of phospholipid substrates with a short *sn-2* chain [1]. Originally the enzyme was identified by its ability to hydrolyze the acetyl group from the *sn-2* position of the signaling molecule platelet-activating factor (PAF), and was therefore referred to as PAF acetylhydrolase [2]. In addition to its suspected role in reducing PAF levels, gVIIA-PLA2 hydrolyzes other pro-inflammatory agents such as oxidized lipids of LDL particles [3,4]. Physiologically, gVIIA-PLA2 is associated with both LDL and HDL particles, and is also referred to as lipoprotein-associated PLA2 (Lp-PLA2) [5]. The enzyme is tightly associated with lipoprotein particles, and is thought to access substrates from both the lipoprotein surface and from the aqueous phase [6–8].

Organophosphorous (OP) compounds are believed to exhibit their toxicity primarily through the inhibition of acetylcholinesterase (AChE), which is responsible for degrading the neurotransmitter acetylcholine. Nerve agents such as sarin, soman, and tabun (Fig. 1) pose a risk to human health. Additionally, a larger

☆ Protein Data Bank entry codes 3F9C, 3F96, 3F97, and 3F98 are non-aged complexes of human group-VIIA phospholipase A2 with the pesticide diisopropylfluorophosphate or the nerve agents sarin, soman and tabun, respectively.

☆☆ This work was supported by NIH Grants 2P20RR015588 from the National Center for Research Resources and 1R01HL084366-A1 from the National Heart, Lung, and Blood Institute. The opinions, interpretations, conclusions, and recommendations are those of the authors and are not necessarily endorsed by the U.S. Army or the Department of Defense.

Abbreviations: AChE, acetylcholinesterase; AH, acetylhydrolase; BChE, butyrylcholinesterase; BOG, *n*-octyl-β-D-glucopyranoside; DFP, *O,O*-diisopropylfluorophosphate; ESI, electrospray ionization; GC, gas chromatography; gVIIa, group-VIIa; gVIII, group-VIII; Lp-PLA2, lipoprotein-associated phospholipase A2; MALDI, matrix-assisted laser desorption ionization; MS, mass spectrometry; *m/z*, mass to charge; OP, organophosphorus; PAF, platelet-activating factor; paraoxon, *O,O*-diethyl-*O*-nitrophenylphosphate; sarin, *O*-isopropyl methylphosphonofluoridate; soman, *O*-pinacolyl methylphosphonofluoridate; tabun, ethyl *N,N*-dimethylphosphoramidocyanidate; TCEP, triscarboxyethylphosphine; VX, *O*-ethyl *S*-2-(diisopropylaminoethyl) methylphosphonothiolate.

* *Corresponding author at*: Department of Chemistry & Biochemistry, University of Delaware, 312 Drake Hall, Newark, DE 19716, USA. Tel.: +1 302 831 0786; fax: +1 302 831 6335.
E-mail address: bahnson@udel.edu (B.J. Bahnson).

0006-2952/$ – see front matter © 2009 Elsevier Inc. All rights reserved.
doi:10.1016/j.bcp.2009.04.018

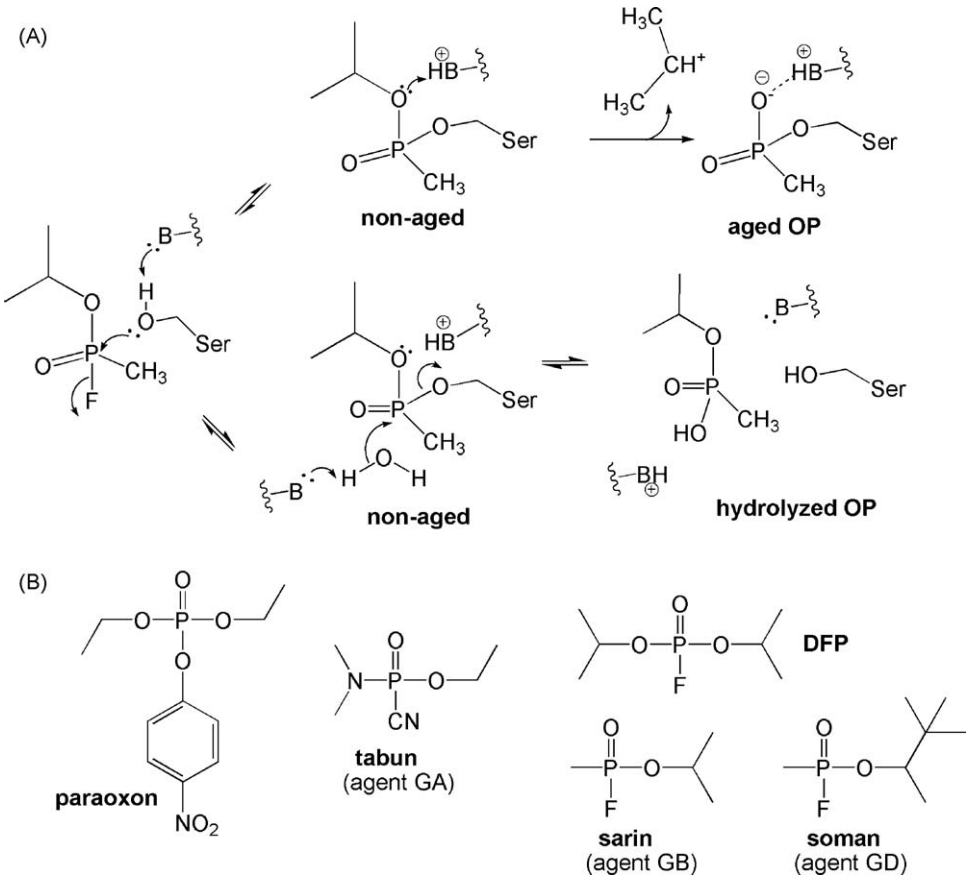

Fig. 1. OP nerve agents react with Ser hydrolases, such as AChE or gVIIA-PLA2. (A) The inhibition of a serine hydrolase with an OP compound, such as *O*-isopropyl methylphosphonofluoridate (sarin, GB) can stop at a non-aged complex, proceed to an "aged" complex through a carbocation mechanism (top branch), or be hydrolyzed to a harmless product (bottom branch). The aging path is promoted by a secondary or tertiary C_α, which stabilizes the developing positive charge. The hydrolysis path is promoted, if aging is not fast, and if a nucleophilic water can approach the non-aged species. (B) The OP compounds sarin, *O*-pinacolyl methylphosphonofluoridate (soman, GD) and *O*,*O*-diisopropylfluorophosphate (DFP) have a branched side chain that facilitates aging, whereas *O*,*O*-diethyl-*O*-nitrophenylphosphate (paraoxon) and ethyl *N*,*N*-dimethylphosphoramidocyanidate (tabun, GA) do not.

superfamily of serine hydrolases, including gVIIA-PLA2, have been shown to be inactivated by OPs, with potential clinical consequences [9]. As depicted in Fig. 1, the nucleophilic serine residue reacts with OPs by a S_N2 mechanism with a trigonal bipyramidal transition state, and stereoinversion occurs at the chiral phosphorus atom [10]. Depending on the enzyme, the initial complex can yield one of several results: reactivation through spontaneous hydrolysis, reactivation with a strong nucleophile, dealklyation of the OP adduct, or maintenance of a stable complex. When bound to AChE, OP compounds with a branched side chain at the C_α adjacent to the phosphoester typically undergo a rapid dealkylation process referred to as aging [11,12]. The aging process in AChE is thought to be irreversible, as the covalently inhibited enzyme cannot typically be reactivated by nucleophiles to regenerate enzymatic activity. Alternatively, the non-aged complex can undergo a reactivation by attack of an activated water molecule or an alternative activated nucleophile (e.g., oxime). Efforts have focused on engineering serine hydrolase enzymes to hydrolyze pesticides and nerve agents, and therefore function as catalytic OP bioscavengers [13]. OP nerve agents such as sarin, soman, tabun or VX are particularly toxic to humans and are commonly referred to as chemical warfare agents. The gVIIA-PLA2 enzyme is an intriguing system to explore OP reactivity, as it is present in human blood, which is the path nerve agents take to their ultimate target of nerve synapse AChE, and the most suitable site for detoxifying OPs under the bioscavenger paradigm.

One approach to develop an OP bioscavenger is to use structures of serine hydrolases complexed with the nerve agents of interest as a starting point to engineer hydrolase activity. Several systems have been examined, which include structural information of both aged and non-aged complexes. Crystal structures exist for non-human AChE complexed with sarin, VX and DFP in both aged and non-aged forms [10,14,15]. Additionally, the non-aged structure of human butyrylcholinesterase (BChE) was reported in complex with the OPs echothiophate [16] and tabun [17]. Although VX and echothiophate have a propensity to age, the leaving group is unbranched at the C_α position, suggesting that this is a relatively slow reaction in both AChE and BChE. More recently, human carboxylesterase was reported to form non-aged complexes with the OPs soman and tabun [18]. Additionally, bovine group-VIII (gVIII)-PLA2 was reported by us to form non-aged complexes with sarin and soman [19].

The gVIIA-PLA2 enzyme, which is structurally, functionally and physiologically unrelated [8] to the gVIII-PLA2 enzyme, is bound to lipoproteins. It has great promise as a potential OP bioscavenger, as it is naturally present in human blood. We recently reported the crystal structure of gVIIA-PLA2 in a ligand-free form and following reaction with the OP insecticide paraoxon [8]. In our present work, we report the structures of gVIIA-PLA2 following reaction with the OP compounds sarin, soman, tabun and DFP to a resolution of 2.1, 1.7, 1.7, and 2.3 Å, respectively. Each structure reported provides convincing evidence of non-aged complexes, and in the case of the tabun complex, a single stereoisomer in the crystal structure. Furthermore, results reported from mass spectrometry experiments corroborate the crystallographic results of non-aged OP

complexes, and show evidence for a lack of stereoselectivity of reaction of sarin with gVIIA-PLA2.

2. Materials and methods

2.1. Preparation of protein

Crystallization experiments utilized human gVIIA-PLA2 (PAFase, residues 47–429, NCBI accession Q13093) which was overexpressed in *E. coli* and obtained from ICOS Corporation. Details of the protein preparation of the ICOS-produced protein and initial crystallization of the ligand-free form of human gVIIA-PLA2 have been reported previously [20]. Mass spectrometry work utilized both PAFase from ICOS and human gVIIA-PLA2 protein expressed in our lab using the following methods. The full-length clone of human gVIIA-PLA2 was purchased from Invitrogen (NCBI accession BC038452), the cDNA was amplified by PCR, and subcloned into the expression plasmid pGEX-4T3 (GE Healthcare) utilizing *Sal*I (Invitrogen) and *Not*I (New England Biolabs) restriction enzyme sites. The recombinant gVIIA-PLA2 construct included residues 42–441 of human gVIIA-PLA2 with an N-terminal extension of 8 additional residues which remained after thrombin cleavage. This construct represents a full-length construct of gVIIA-PLA2. The N-terminus start of gVIIA-PLA2 found in human blood is heterogeneous, with a mixture of N-termini at positions Ser35, Ile42 or Lys55 [2]. The natural C-terminus of gVIIA-PLA2 is residue Asn441. The first eight amino acids of this construct (GSPNSRVD) are non-native sequence coming from the multiple cloning site of the PGEX4T-3 vector into which the gVIIA-PLA2 sequence was cloned. The GST-gVIIA-PLA2 fusion protein was over-expressed in *E. coli* strain BL21. Ten milliliters of the overnight culture was inoculated into 1 l of fresh LB media containing 75 μg/ml ampicillin (Sigma–Aldrich) and grown at 37 °C until an optical density of 0.5–0.6 was reached at 600 nm. Protein expression was induced by the addition of 0.5 mM IPTG (Sigma–Aldrich) at 37 °C for 4 h. Cells were harvested by centrifuging at 5000 rpm for 10 min at 4 °C. Cells were lysed by sonication in 50 mM Tris (Fisher Sci.), pH 7.8, 100 mM NaCl (Fisher Sci.), 5 mM DTT (Sigma–Aldrich), 1 mM PMSF (Sigma–Aldrich), 0.1 mg/ml lysozyme (Sigma–Aldrich). Cell lysis was followed by detergent extraction with 0.2% (w/v) Triton DF-16 (Sigma–Aldrich) for 30 min at 4 °C. The fusion protein was purified by affinity chromatography using glutathione sepharose (GE Healthcare). The GST-tag was cleaved from the fusion protein via on-column cleavage using thrombin protease (Enzyme Research Laboratories). Digestion was typically allowed to proceed overnight at 4 °C. After digestion, cleaved gVIIA-PLA2 was eluted with 50 mM Tris, pH 7.8, 500 mM NaCl, 1 mM EDTA (Sigma–Aldrich), 1 mM DTT, 0.2% (w/v) Triton DF-16. Thrombin was removed from the purified protein by affinity chromatography using a benzamidine sepharose cartridge column (GE Healthcare). Purified protein was concentrated to 3–4 mg/ml using centrifugal filter units (Millipore). Concentrated protein was dialyzed against 50 mM Tris, pH 7.8, 100 mM NaCl, 1 mM EDTA, 1 mM DTT, 0.2% (w/v) Triton DF-16 before storage at 4 °C.

2.2. Inhibition and crystallization of gVIIA-PLA2

Samples of gVIIA-PLA2 (PAFase, residues 47–429) were prepared for crystallization as previously described [20] and concentrated to 4 mg/ml. The enzyme was subsequently incubated with a 4-fold molar excess of racemic sarin, soman or tabun provided by the U.S. Army Medical Research Institute of Chemical Defense (Aberdeen Proving Ground, MD) under controlled engineering conditions. After inhibition with OPs, the enzyme samples were incubated overnight at 4 °C, and activity was measured with the substrate *p*-nitrophenylacetate (Sigma–Aldrich) to ensure a lack of enzymatic activity. The crystallization conditions for the ligand-free [8,20] and paraoxon complexed form [8] of gVIIA-PLA2 have been reported previously. For the crystallization of sarin and soman-inhibited protein, the stock included: 4 mg/ml inhibited protein, 10 mM Tris–HCl, 6 mM sodium citrate, 3% (w/v) sucrose, 1.0 mM DTT, 27 mM *n*-octyl-β-D-glucopyranoside (BOG), 0.04% (w/v) pluronic F68, 0.002% (w/v) Tween 80, pH 6.7 (materials from Sigma–Aldrich). The reservoir solution for the crystallization of the sarin complex contained 40% $(NH_4)_2SO_4$ (w/v), 0.4 M Li_2SO_4, 1.1 M Na^+-formate, pH 7.0, 1.4% 1,4-butanediol (v/v) (materials from Sigma–Aldrich). The reservoir solution for crystallizing a soman-inhibited complex contained 0.1 M MOPS buffer, pH 6.6, 43% (w/v) $(NH_4)_2SO_4$, 0.4 M Li_2SO_4, 1.0 M sodium acetate, and 1.48% (v/v) 1,4-butanediol (materials from Sigma–Aldrich). Aliquots of 1.5 μl of protein and crystallization solutions were mixed to form each hanging drop, and protein crystals formed within 4 weeks at 20 °C and were allowed to grow over several more weeks. The protein composition for crystallization of tabun-inhibited protein was similar to that for sarin and soman, but the reservoir composition contained 0.1 M MOPS, pH 6.6, 37% $(NH_4)_2SO_4$, 0.4 M Li_2SO_4, 1.2 M Na^+-formate, pH 7.0 and 1.3% 1,4-butanediol. Aliquots of 1.5 μl of protein and crystallization solutions were mixed to form each hanging drop, and protein crystals formed within 3–4 weeks and were grown for an additional several weeks. Crystals of inhibited protein were flash frozen directly from the crystallization drop into liquid nitrogen, which allowed facile transport to the synchrotron beam line. Crystals were flash cooled without the need of an additional cryoprotectant. The treatment of DFP-inhibited protein crystals varied. Initially ligand-free protein crystals of gVIIA-PLA2 were grown by the methods described previously [8]. Then crystals were transfered into a reservoir solution containing 27 mM BOG, 1.0 mM DTT and a 4 mM DFP solution. Protein crystals were soaked in this DFP solution for 20 min, and then flash frozen into liquid nitrogen.

2.3. Crystal structures of OP complexes

X-ray diffraction data for tabun gVIIA-PLA2 crystals were collected at beam line 19ID, whereas gVIIA-PLA2 sarin and soman complex crystal data were collected at beam line 24ID of the Advanced Photon Source at the Argonne National Laboratory. The DFP-inhibited protein X-ray diffraction data were collected with a Rigaku RU-H3R anode generator and a RAXIS IV image plate area detector of our in-house system. The program HKL2000 [21] was used to process data in the space group *C*2 for complexes of sarin, soman and DFP, and the tabun-inhibited complex data were processed in the space group of $C222_1$. The structure of gVIIA-PLA2 (PDB entry 3D59) [8] was used as a starting model for molecular replacement minus water molecules and ions. Molecular replacements were carried out using the program MOLREP of CCP4 [22] and refinements of each OP complex were accomplished using the program REFMAC5 of CCP4 [22]. Model building and modification were done using the graphics program COOT [23]. The final molecular replacement solutions consisted of two subunits in the asymmetric unit for sarin, soman and DFP complexes, whereas for the tabun complex there were three molecules per asymmetric unit. Extra difference electron density contiguous with the active site residue Ser273 was identified in $2F_o - F_c$ difference electron density maps in all four complexes and determined to be the covalently attached OP inhibitor. In all cases there was unambiguous difference electron density of the proper configuration to build in non-aged OP adducts. Since the sarin used was racemic, the resulting inhibited complex could potentially have one or both of two possible stereoisomers (P_R and P_S) at the P-chiral center. Soman, which has two chiral centers, had the potential to have four

stereoisomers (P_RC_R, P_RC_S, P_SC_R and P_SC_S) in the crystal structure. We have modeled the P_R and P_S forms at the P-center of the sarin conjugate with the occupancy of each set to 0.5. And likewise for soman, the P_RC_S and P_SC_S forms were modeled with an occupancy of each set to 0.5. The tabun compex was modeled in only the P_S conformation, as this form dominated in the crystal structure. For DFP the achiral complex was modeled. Models were refined with the program REFMAC5 [24]. A CIF parameter file for the non-aged complexes formed after reaction with sarin, soman, tabun, and DFP was prepared using the monomer library sketcher module of the program CCP4 [22].

2.4. Mass spectrometry of trypsin digests

Although the crystallographic data gave convincing evidence for the presence of non-aged complexes with soman, an additional confirmation of the presence of a non-aged complex was sought via mass spectrometry analysis of peptides formed by trypsin digestion of soman-inhibited gVIIA-PLA2 to detect modification at the active site serine (Ser273). Matrix-assisted laser desorption ionization mass spectrometry (MALDI-MS) analysis was done on soman inactivated complexes of gVIIA-PLA2. Soman was chosen for the mass spectrometry investigation since it is a branched OP that is known to age at a fast rate in complexes with AChE and BChE [25].

Inhibition of gVIIA-PLA2 with soman was performed at the U.S. Army Medical Research Institute of Chemical Defense as described above for the inhibition of protein crystals. The inhibition of gVIIA-PLA2 was accomplished by adding 1 μl of a 10 mM stock of soman in saline to 10 μl aliquots (0.7 mg/ml) of gVIIA-PLA2 in 10 mM Tris, pH 8. Inhibition of gVIIA-PLA2 with soman was relatively slow compared to the cholinesterases, and was confirmed by assaying enzyme activity using the substrate *p*-nitrophenylacetate. Inhibited gVIIA-PLA2 was incubated at 4 °C for at least 48 h before proceeding to trypsin digestion.

Samples were buffer exchanged into 50 mM ammonium bicarbonate using BioGel P-4 micro spin buffer exchange columns (BioRad) to remove any residual OP compound that could interfere with trypsin digestion. All samples, including an uninhibited control sample, were separated by SDS-PAGE electrophoresis, stained with 0.1% Coomassie blue, and isolated by excision of selected protein bands. In-gel digestion was performed using Zip Plates with the MultiScreen HTS vacuum manifold (Millipore, Billerica, MA). Each gel piece was washed, dried, reduced by treatment with 10 mM DTT and alkylated by treatment with 55 mM iodoacetamide (Sigma–Aldrich). The treated gel spot was dried and rehydrated in 25 mM ammonium bicarbonate containing 11 ng/μl trypsin (Pierce) and incubated at 37 °C overnight. Peptides were eluted in 20 μl matrix solvent (50% acetonitrile/0.1% trifluoroacetic acid/1 mM ammonium phosphate), dried completely in a vacufuge and stored at −20 °C until ready for analysis by MALDI-MS.

2.5. Identification of proteins by MALDI-MS

The dried peptide fragments were resuspended in 2–5 μl matrix solution (2.5 mg/ml α-cyano-4-hydroxycinammic acid; Sigma–Aldrich) in matrix solvent (50% acetonitrile/0.1% trifluoroacetic acid/1 mM ammonium phosphate). The resuspended peptides were spotted on a stainless steel target plate. The sample was analyzed using a MALDI tandem Time-of-Flight (ToF-ToF) 4700 Proteomics Analyzer (Applied Biosystems). Data acquisition by the instrument was controlled with 4000 Series Explorer Software v3.0, acquiring spectra using delayed extraction and reflectron mode with positive ion detection. GPS Explorer Software v3.5 with Mascot was used to identify proteins by peptide mass fingerprinting. Interpretable mass spectra with high sequence coverage were obtained for all peptide fragments.

2.6. Analysis of stereoselectivity by reaction with racemic sarin

We studied the stereoselectivity of plasma gVIIA-PLA2 for specificity in binding the stereoisomers of sarin by tandem gas chromatography/mass spectrometry (GC/MS) using methods modified from Yeung et al. [26]. Assays were performed at the U.S. Army Medical Research Institute of Chemical Defense, Aberdeen Proving Grounds under controlled conditions. For sarin binding, a 50 μl sample of purified gVIIA-PLA2 (~66 nM) or buffer (10 mM potassium phosphate, pH 7.4) was incubated for 30 min at room temperature with 815 nM racemic sarin. At each time point during the incubation, a 100 μl sample was extracted with an equal volume of dry ethyl acetate supplemented with 50 μM DFP as an internal standard. The organic layer (60 μl) containing the unbound sarin was removed and passed over type 4A (grade 514) alumina-silicate molecular sieves to remove excess water. Forty microliters of this dry sample was transferred to 11 mm crimp top vials for GC/MS analysis. One μl samples were autoinjected and passed through an Agilent 6890 gas chromatograph fitted with a 20 m × 0.25 mm inside diameter Chiraldex gamma-cyclodextrin trifluoroacetyl column with 0.125 μm film thickness (Advanced Separation Technologies Inc.). The GC was interfaced to an Agilent 5973 mass spectrometer with an electronic impact ion source under selected ion monitoring mode. The mass to charge (m/z) peaks at 99 and 125 were monitored for sarin quantitation. The OP compound DFP was used as an internal standard, and its concentration was monitored with three ions (m/z 69, 101 and 127). The total area under the curve was used to develop ratios of each isomer between samples.

3. Results

3.1. Crystal structures of organophosphorus complexes of gVIIA-PLA2

The refined models of OP complexes of gVIIA-PLA2 following inactivation with DFP, sarin, soman and tabun each have a typical α/β lipase fold virtually identical to the previously reported ligand-free and paraoxon bound forms [8]. The details of the data collection and structural refinement for all four complexes are summarized in Table 1. The DFP, sarin and soman complexes were solved in the space group *C*2 with two subunits in the asymmetric unit. This packing was isomorphous to the ligand-free and paraoxon bound form previously reported [8]. The tabun inactivated complex crystallized in a new space group ($C222_1$) and had three subunits in the asymmetric unit. The enzyme is believed to function as a monomer [7,8]; yet the crystal structures reported here have fairly extensive inter-dimer or inter-trimer interfaces, as shown in Fig. 2 for the soman and tabun complexes, respectively.

The sarin gVIIA-PLA2 complex was modeled with residues 54–425 in subunit A and 54–426 in subunit B; a few residues at the N-terminus (47–53) and C-terminus (426–429 in A and 427–429 in B) were not modeled due to disorder. The soman complex was modeled with residues 54–425 in both subunits and N- and C-terminal residues were not modeled due to disorder. The DFP complex was modeled with residues 54–425 in subunit A, and 54–426 in subunit B. The tabun complex was solved from a different space group, which contained three subunits per asymmetric unit. Additionally, an unusual CH···π interaction between the *N*,*N*-dimethyl group of the tabun conjugate in subunit A and Phe51 of subunit C increased the order of the N-terminal resides. The tabun complex was more ordered than the other complexes, with five additional residues modeled at the N-terminal compared to each of

Table 1
Structure determination of OP complexes of gVIIA-PLA2.

Data set	Sarin	Soman	Tabun	DFP
Beam line	ASP-24ID	APS-24ID	APS-19ID	RAXIS-IV
Space group	*C*2	*C*2	*C*2221	*C*2
Unit cell dimensions: *a*, *b*, *c* (Å), β (°)	116.1, 82.5, 96.6, 115.1	116.1, 82.7, 96.7, 115.3	77.0, 133.3, 253.9, 90.0	116.4, 82.4, 96.5, 115.6
Subunits/asymmetric unit	2	2	3	2
Wavelength	0.9795	0.9795	1.0055	1.5418
Resolution (Å)	50–2.1 (2.18–2.10)	50–1.7 (1.76–1.70)	50–1.7 (1.76–1.70)	50–2.30 (2.38–2.3)
Number of frames	400	360	480	201
Oscillation	0.5	1.0	0.5	1
Temperature	100 K	100 K	100 K	100 K
R_{merge} (linear)[a]	0.083 (0.264)	0.057 (0.261)	0.070 (0.435)	0.069 (0.44)
$I/\sigma I$	11.2 (1.9)	20.0 (2.4)	35.0 (5.6)	20.7 (3.2)
Completeness (%)	96.1 (73.1)	96.4 (73.1)	98.8 (97.8)	100 (100)
Redundancy	3.6 (1.9)	3.7 (1.9)	10.0 (10.1)	4.2 (4.1)
Refinement				
Resolution (Å)	50.0–2.10	50.0–1.70	50.0–1.70	50–2.3
Total reflections	45,826	87,071	141,507	36,675
$R_{working}/R_{free}$[b]	0.2098/0.2777	0.1832/0.212	0.1801/0.2017	0.203/0.265
Number atoms				
Protein	5988	6018	9352	5978
Water	196	389	1084	170
Other	12	53	282	20
B-factor				
Protein	36.4	23.9	17.8	34.7
Main chain atom	35.4	22.6	16.8	34.1
Side chain atoms	37.3	25.1	18.7	35.3
RMS from ideal values				
Bond lengths (Å)	0.02	0.01	0.01	0.02
Bond angles (°)	1.90	1.33	1.35	1.81
Ramachandran plot (most-favored)	90%	91.2%	92.7%	90.0%
Ramachandran plot (most-favored and additional allowed region)	100%	99.6%	99.7%	99.7%
PDB code	3F96	3F97	3F98	3F9C

[a] $R_{merge} = \sum|I_o - I_a|/\sum(I_a)$, where I_o is the observed intensity and I_a is the average intensity, the sums being taken over all symmetry related reflections.
[b] *R*-factor = $\sum|F_o - F_c|/\sum(F_o)$, where F_o is the observed amplitude and F_c is the calculated amplitude. R_{free} is the equivalent of $R_{working}$, except it is calculated for a randomly chosen set of reflections that were omitted (5%) from the refinement process [40]. Values shown in the parenthesis are in the highest resolution shell.

the other gVIIA-PLA2 structures solved to date. There are several surface loop residues in each of the structures that were modeled with alternate conformations. The overall quality of each complex structure is very good as demonstrated by the percentage of residues in most favored and additionally allowed regions of Ramachandran plot (Table 1). A comparison between the ligand-free and OP complex crystal structures shows an overall C_α RMSD of 0.31 Å for DFP, 0.28 Å for sarin, 0.25 Å for soman, and 0.50 Å for tabun, which indicates the structures of OP complexes are essentially identical to that of the ligand-free protein structure [8].

3.2. DFP complex with gVIIA-PLA2

Sufficient quality difference electron density was present to model in the entire serine-phosphonyl diisopropyl covalent species. The model of the DFP complex with gVIIA-PLA2 is highly similar to the complex formed following reaction with the OP paraoxon [8] and is presented in supplemental-Fig. 1A. Several interactions between the inhibitor and the enzyme have been observed and are listed in Table 2 for each OP complex presented. The double bonded phospho-oxygen is interacting with the oxyanion hole of the enzyme through H-bonds to the backbone amides of Phe274 and Leu153. His351 is seen making a H-bond with the phosphoester oxygen of this substituent where His351 is unable to activate a water molecule for catalytic turnover. Presumably, His351 is protonated as a result of proton abstraction from Ser273 concurrent with nucleophilic attack on DFP. This direct H-bond interaction precludes His351 from reverting to an unprotonated form and activating a water molecule for a nucleophilic attack, which could reactivate the enzyme.

In the DFP complex, one isopropyl group projects toward the solvent channel, which is close to the catalytic His351, and the other isopropyl group is away from histidine; the oxygen to His351 distances are 2.99 and 4.07 Å, respectively. None of the oxygen atoms attached to isopropyl groups are accessible to the solvent water and their solvent accessibility becomes almost zero in the complex. Here, the orientation of the alkyl groups have made water inaccessible to the P atom of the OP conjugate as well. Additionally, a lack of water accessibility to His351 suggests the histidine-assisted activation of water for aging is not likely in this complex. Therefore aging through either P–O bond or C–O bond cleavage is not feasible, and the complex is clearly not aged in the crystal structure. The double bonded phospho–oxygen is interacting with the oxyanion hole of the enzyme through H-bonds to the backbone amides of Leu153 and Phe274. Although the contact distances of the neighboring residues to Ser273 are greater than those observed in the ligand-free structure of the enzyme, other geometrical parameters of neighboring residues are essentially the same in order to maintain the structural integrity of the enzyme.

3.3. Sarin complex with gVIIA-PLA2

The model of the gVIIA-PLA2 sarin complex shares many of the interactions discussed above for the DFP complex structure. However, there are a few interesting details worth noting. Sarin has two stereoisomers due to the chiral center at P. There appear to be both stereoisomers of the P-center bound to the enzyme at equal occupancy, and modeled accordingly with an occupancy of 0.5 during refinement of the structure. The racemic model of sarin bound to gVIIA-PLA2 is presented in supplemental-Fig. 1B. When

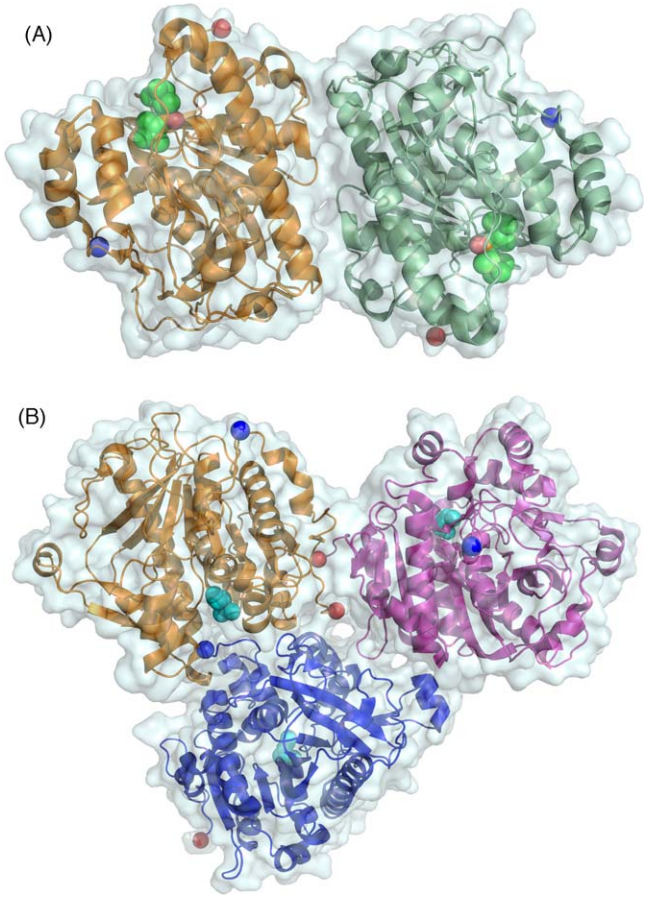

Fig. 2. Surface and ribbon diagram of the soman-dimer and tabun-trimer crystal structure complexes with gVIIA-PLA2. The N- and C-termini of each subunit are depicted with a blue and red sphere, respectively. (A) The soman complex and Ser273 atoms are shown as green CPK spheres. The A and B subunits are shown in orange and green, respectively. (B) The tabun complex and Ser273 atoms are shown as blue CPK spheres. The A, B and C subunits are shown in orange, red and blue, respectively. This figure was made with the program PyMol [41].

the DFP and sarin complex structures are superimposed, the placement of the isopropyl group of sarin from each stereoisomer (P_R and P_S) overlaps the two isopropyl groups which exist in the DFP gVIIA-PLA2 complex. The linker oxygen between Ser and P is invariant and has its occupancy set at 1.0 during refinement. Likewise, the double bonded phospho–oxygen, which is interacting with the oxyanion hole of the enzyme through H-bonds to the backbone amide of Leu153 and Phe274, also maintained an occupancy of 1.0. Therefore, in order to model the two distinct stereoisomers at the P-center (P_R and P_S), the methyl and the oxy-isopropyl group attached to P were interchanged and their occupancies were maintained as 0.5 for each alternate conformation. The projection of the oxy-isopropyl group in P_R stereoisomer was the same as that in the DFP complex structure and that was near the catalytic histidine, whereas the oxy-isopropyl group of the Ps isomer was away from His351 and similar to the second oxy-isopropyl group seen for the DFP complex structure. The contact distance of the neighboring residues to Ser273, which is attached to the OP, is almost the same as they are in the ligand-free structure.

3.4. Soman complex with gVIIA-PLA2

The gVIIA-PLA2 soman complex exhibits many of the features of DFP and sarin complexes. However, soman has a total of four stereoisomers due to chiral centers at the P, as well as the C_α of the pinacolyl group. In the crystal structure it was not possible to refine the four different stereoisomer conformations that are likely present, based on our observation of GC mass spectrometry data (see below). In the final structure we have modeled two stereoisomers, the P_RC_S and P_SC_S conformations with the occupancy set at 0.5 for each. The presence of P_R and P_S stereoisomers, shown in Fig. 3A, clearly indicates that the soman complex does not age. As mentioned above for the sarin complex, the solvent accessibility of the conjugate oxygen atoms close to His351 or P is hindered by the large pinacolyl alkyl group. Similar to the sarin complex, the contact distances of the residues neighboring Ser273 in the soman complex are nearly the same as they are in the ligand-free structure.

3.5. Tabun complex with gVIIA-PLA2

Unlike the ligand-free enzyme or other OP complexes, the gVIIA-PLA2 tabun crystallized as a trimer in the asymmetric unit. The S_N2 reaction by Ser273 followed by removal of a cyanide-leaving group, as shown in Fig. 3B, made this complex chiral with the formation of a P_R complex. Despite the inversion at the P-chiral center, the P_R adduct is derived from the reaction of P_R tabun due to the loss of the CN group and nomenclature rules (Fig. 3B). An interesting change in this structure occurs as the electronic effect of *N*,*N*-dimethyl group displaced the active site His351 away from its native and functional conformation. In its present conformation H-bonding is not possible to stabilize the transition state for the aging process. In this non-aged tabun complex extra stability comes from a CH···π interaction between the *N*,*N*-dimethyl group and Phe322 and Trp298 of subunit A, and Phe51of subunit C [27–29]. Like the DFP complex presented above, the contact distances of immediate neighboring residues to Ser273 are greater than

Table 2
OP complex contacts within 4 Å.

Residue/atom type	DFP contact atom, distance (Å)	Sarin[a] contact atom, distance (Å)	Soman[a] contact atom, distance (Å)	Tabun contact atom, distance (Å)
F51C, CZ[b]	–	–	–	C2, 3.47
G152A, CA	O3P, 3.17	O1, 3.54	C3, 3.13	O1, 3.37
L153A, N[c]	O3P, **2.57**	O1, **2.65**	O11, **2.76**	O1, **2.62**
A155A, CB	–	–	C3, 3.78	–
Y160A, OH	C3′, 3.75	–	C3, 3.34	C4, 3.94
H272A, CE1	–	C4, 3.70	C2, 3.20	C4, 3.78
F274A, N	O3P, **2.65**	O1, **2.74**	O11, **2.97**	O1, **2.72**
W298A, CE3	–	C1, 3.71	–	C1, 3.68
F322A, CE1	–	–	–	C2, 3.68
H351A, NE2	O2P, **2.99**	O2, **2.91**	OH, **3.11**	O2, 3.53
Q352A, NE2	C2′, 3.51	C3, 3.98	C2, 2.91	C4, 3.69

[a] For P_SC_S stereoisomer of soman and P_S stereoisomer of sarin.
[b] Residues are defined with single letter code, residue number and subunit relative to OP complexes in the A-subunit of each structure.
[c] Hydrogen bond contacts are shown in bold.

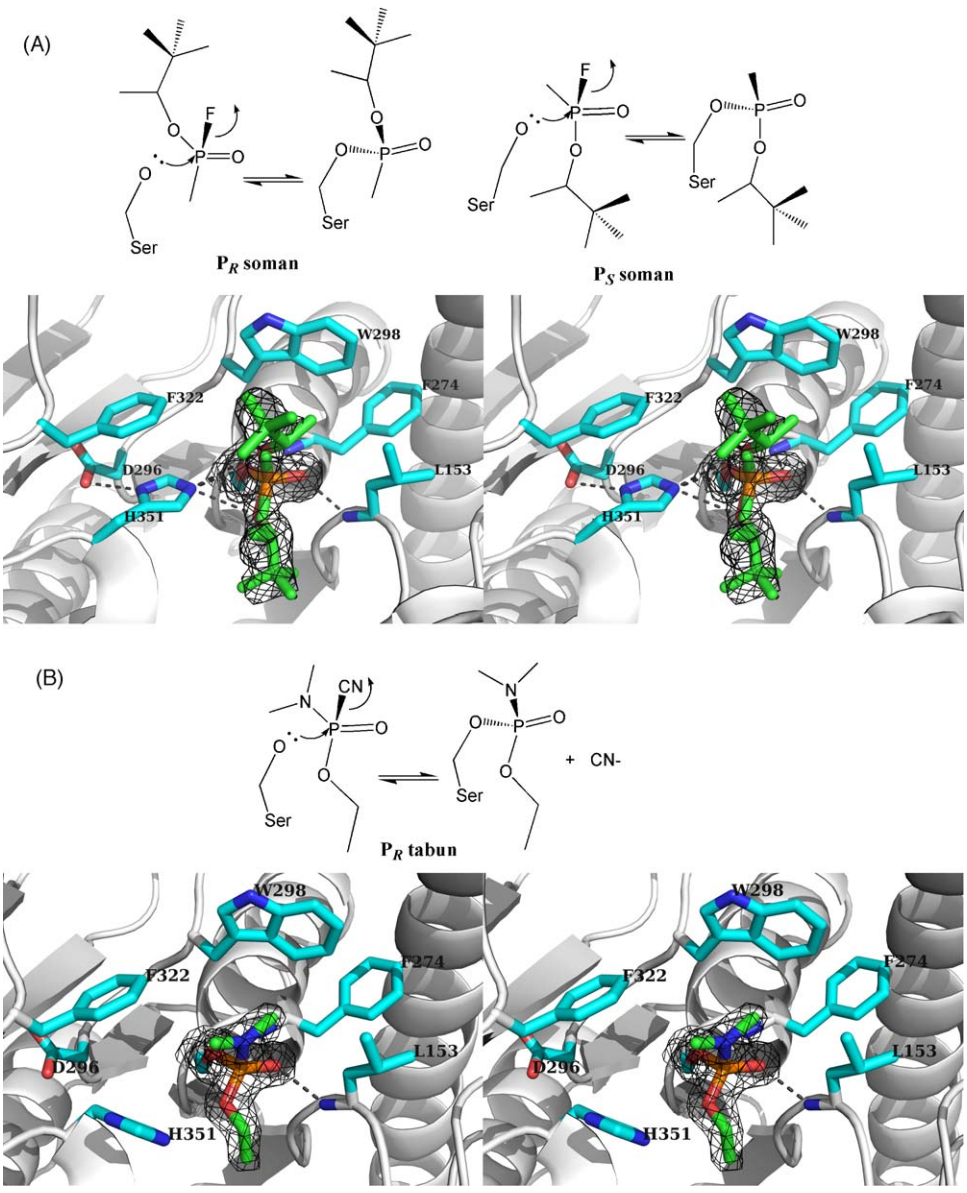

Fig. 3. The reaction of gVIIA-PLA2 with soman and tabun to Ser273 are shown relative to active site residues Phe322, Trp298, Phe274, Leu153, Asp296 and His351. The catalytic triad is composed of Ser273, His351 and Asp296; and the oxyanion hole is formed by H-bond interactions with the amide-N of Phe274 and Leu153. (A) Both the P_S and P_R stereoisomers of soman reacted to give racemic adducts covalently attached to Ser273 of the enzyme. A stereoview (walleye) of the active site is displayed with a difference electron density map ($2F_o - F_c$ coefficients, 1.0σ) around the soman adduct, which demonstrates the lack of a stereochemical preference of the inactivation. The P_S and P_R soman stereoisomers, which were modeled simultaneously (green), were refined with each stereoisomer set to 50% occupancy. (B) The P_R stereoisomer of tabun reacted to give the P_R adduct covalently attached to Ser273 of the enzyme. Despite the inversion at the P-chiral center, the adduct remains P_R due to the loss of the CN group and nomenclature rules. A stereoview (walleye) of the active site is displayed with a difference electron density map ($2F_o - F_c$ coefficients, 1.2σ) around the tabun adduct, which demonstrates the stereochemical preference of the inactivation. This figure was made with the program PyMol [41].

those observed in the ligand-free structure of the enzyme. Other geometrical parameters of neighboring residues are essentially the same, thus maintaining the structural integrity of the enzyme.

3.6. Mass spectrometry analysis of OP-inhibited gVIIA-PLA2

While the electron density maps of the gVIIA-PLA2 soman and sarin complexes were highly suggestive of full occupancy of non-aged inhibitor, analysis via mass spectrometry was pursued as further proof and to ensure that the difference electron density maps were not being misinterpreted. Uninhibited plasma gVIIA-PLA2 along with enzyme inhibited by soman were subjected to trypsin digestion and MALDI-ToF MS analysis. The peptide fragment generated after trypsin digestion containing the active site serine (Ser273) has the predicted sequence 267–IAVIGHSFG-GATVIQTLSEDQR–288 with an expected mass of 2299.548 Da. The peptide was observed in both the untreated and soman-inhibited samples, although its abundance was dramatically decreased in the soman-inhibited sample. The MALDI mass spectra are presented in supplemental-Fig. 2. Table 3 lists the key detected peptide peaks with masses equal to and greater than the Ser273 peptide. We observed three new peptide masses after soman inhibition, which correspond to the addition of 48.97, 83.96 and 162.10 Da to the Ser273 peptide. The addition of 162 Da is the change in mass predicted for the addition of a soman molecule after loss of its fluoride-leaving group upon binding. If an OP aging event occurred, we would expect the total mass addition to be only 78 Da after loss of the secondary alkoxy-leaving group. No

Table 3
MALDI masses of a Ser273 peptide before and after modification with soman.[a].

Ser273 peptide *m/z*	*m/z* increase	Ser273 peptide + soman *m/z*
2299.237		2299.234
2316.218		2316.216
2326.185		2326.177
2332.205		2332.202
	+48.97	2348.201
2351.208		2351.199
2357.244		2357.233
2358.229		2358.221
2364.179		2364.183
	+83.96	2383.192
2440.338		2440.337
	+162.10	2461.330
2542.392		2542.398

[a] The MALDI *m/z* masses are shown for a Ser273 peptide (267–288) from a trypsin digest of gVIIA-PLA2 pre- and post-incubation with soman. For the soman treated sample, fragments that are unique from the untreated sample have the increase of mass designated. The *m/z* peak (mass increase +162.10) of 2461.330 is consistent with a non-aged complex of soman with the enzyme. The *m/z* peaks with mass increases of +48.97 and +83.96 have not been assigned, but do not correspond with a *m/z* peak of +78 that would be expected for an aged species. The absence of a *m/z* peak with an increase of +78 supports the lack of soman aging for the gVIIA-PLA2 complex. This portion of the mass spectrum of each sample is shown in supplemental-Fig. 2.

fragment from the inhibited peptide pool was observed which corresponded with a mass 78 Da greater than the uninhibited peptide. The presence of a peak consistent with a non-aged adduct at 2461.330 Da and the absence of a peak of the size predicted for an aged product further support the identity of a non-aged soman adduct in our complexes. The unmodified plasma gVIIA-PLA2 sample showed a major peak consistent with the predicted mass of an unmodified Ser273, and the soman-inhibited protein spectra is likewise consistent with the identity of a non-aged enzyme complex (supplemental-Fig. 2).

3.7. Analysis of stereoselectivity by reaction with racemic sarin

We studied stereoselective binding of sarin to gVIIA-PLA2 and ICOS PAFase (Fig. 4) by GC/MS using a chiral column to separate the two stereoisomers of sarin (P_S and P_R). Prior experiments that reacted sarin with human BChE have enabled us to assign the second peak as the P_S stereoisomer of sarin (not shown). We observed bulk binding of sarin to both ICOS and recombinant gVIIA-PLA2, which was observed by the decrease in the peak area compared to the control of sarin in buffer. There was no stereoselective preference for binding of either sarin isomer. ICOS PAFase was tested in parallel with similar results. This qualitative result is consistent with the crystallographic data, which likewise supports the lack of preference of gVIIA-PLA2 for either stereoisomer of sarin.

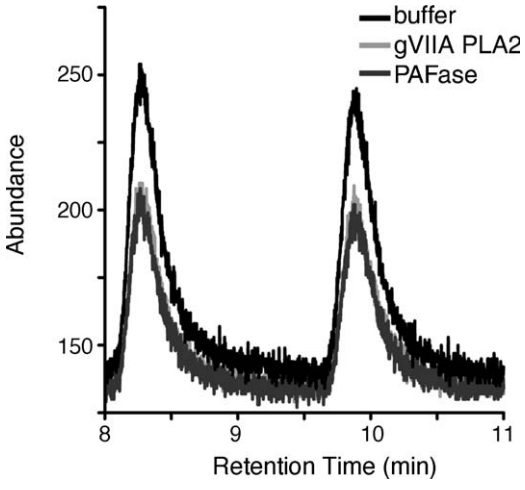

Fig. 4. Analysis of the reaction of gVIIA-PLA2 with sarin. The control (top black trace) is an injection of sarin in buffer only. The control and two forms of gVIIA-PLA2 enzyme reacted samples (recombinant gVIIA-PLA2, light gray trace; and ICOS PAFase, dark gray trace) were incubated with racemic sarin for 30 min at room temperature before extraction and isolation of the unbound sarin. The traces show the abundance of each stereoisomer as a function of column retention time. There was virtually no difference between the two enzyme forms as shown by the nearly superimposed lower traces. Note that the data were normalized relative to DFP as an internal standard.

4. Discussion

Although structures of gVIIA-PLA2 inhibited by OPs do not definitively serve in identifying the physiological substrates of the lipoprotein-associated enzyme, they do provide clues to important interactions of the putative hydrolase mechanism. Here the OP-inhibited structures help to further describe the limits of the possible modes of substrate binding. The previously reported crystal structure of gVIIA-PLA2 inhibited by the OP compound paraoxon [8] allowed us to predict how a substrate would access and bind to the active site. This covalent complex served as a tetrahedral intermediate mimic of the esterolysis reaction, and allowed us to substitute the paraoxon derived diethyl phosphate conjugate from our crystal structure with a speculative model of the tetrahedral intermediate of the physiological PLA2 reaction of phospholipid with a short *sn-2* chain. It was predicted that the larger lyso-moiety, which would be the leaving group from the collapse of the tetrahedral intermediate, projects out of the active site toward the solvent and polar portion of the interface. A smaller pocket projects inward that has been modeled with the *sn-2* chain of the substrate. Although this pocket may limit the size of the *sn-2* chain of substrates, and thereby explain the enzyme's preference for a shortened and polar *sn-2* chain [4,6,7], it is a fairly open pocket that could accommodate larger chains. Our structures of gVIIA-PLA2 complexed with conjugates derived from DFP, sarin and soman reinforce this model. The DFP complex structure has two isopropyl groups, which overlay where the diethyl groups of the paraoxon complex were modeled. The preference of each of these pockets to bind an isopropyl group is better illuminated by the racemic nature of binding in the sarin complex. Here the isopropyl group has adopted a nearly 50/50 distribution between these two pockets, and the smaller methyl group of sarin does as well. When you compare the DFP and sarin complex structures (supplemental-Fig. 1), the binding of these isopropyl groups into both of these pockets would be the expected result. Furthermore, the racemic binding of the soman conjugate (Fig. 3) shows that a larger pinacolyl group binds to each of the two pockets with nearly equal affinity.

The observation of fully interpretable electron density difference maps (coefficients $2F_o - F_c$) for both isopropyl groups of DFP, with the occupancy set at 1.0, is evidence that the complex does not go through the aging process, which would lead to the P–O bond cleavage of one of the isopropyl groups. Likewise, a resistance of the OP conjugate to aging was observed by the racemic modeling of sarin and soman, modeled at 0.5 occupancy in alternate conformations with isopropy and pinacolyl groups, respectively. The stability of the non-aged conjugates of sarin, soman and tabun was demonstrated by the long incubation period of protein co-crystallization of 4–7 weeks at 20 °C. The DFP complex crystal was formed by soaking pre-grown crystals for ~20 min. Further support for a stable non-aged complex of the soman conjugate was shown by MALDI-MS of trypsin digests of soman-inhibited gVIIA-PLA2 enzyme. When samples were compared pre- and post-treatment with soman, a peptide containing Ser273 was shifted to

a mass consistent with a non-aged complex with soman. The decrease of the unmodified peak, as well as the lack of a peak consistent with an aged conjugate, strengthens our conclusion that the soman complex did not show any detectable aging reaction.

Many serine hydrolases have been demonstrated to promote the aging reaction when reacted with branched OPs, such as trypsin with DFP [30], or AChE complexes with sarin, soman or DFP [31]. Each of these enzymes shares the common element of a catalytic histidine to carry out proton transfer and a solvent accessible active site. Recently two enzymes have been shown to be resistant to aging of branched OP complexes; non-aged crystal structures have been reported of human carboxylesterase complexed to soman and tabun [18], and gVIII-PLA2 complexed with sarin and soman [19]. A comparison of the enzyme complexes reported here to both enzymes that have rapid OP aging, as well as those that do not, is instructive to understand the determinants of aging. The most notable explanations of rapid aging rates in the AChE enzyme are due to (i) the mobility of the histidine in the AChE enzyme has been argued to be critical to explain its broad specificity and rapid rates of reaction [15]; (ii) a cation–π interaction of Trp86 in AChE is believed to stabilize a carbocation intermediate [32]; and (iii) the oxygen adjacent to the developing carbocation intermediate of the aging reaction is at least partly water accessible. When one compares the gVIIA-PLA2 enzyme to AChE under these criteria the following observations can be made. The histidine may not have the same degree of mobility as in the AChE enzyme. The OP complexes with DFP, sarin and soman show the histidine to be restricted in movement by the surrounding residues and the alkyl groups of the bound OP conjugate. The complex formed by reaction with tabun was different, and in this case His351 was completely displaced away from a mechanistically significant position (Fig. 3B). Next, the active site of gVIIA-PLA2 contained a tryptophan residue analogous to Trp86 in AChE, which could provide the critical cation–π interactions with a developing carbocation intermediate. However, the geometric positioning of this interaction is not identical and may preclude its utility. This positioning may be critical, as aging rates have been previously rationalized based on the ability of the developing carbocation to be directly stabilized by the enzyme active site [33]. Therefore, it is reasonable to assume that the dielectric of the surroundings and the presence or absence of cation–π interactions would be a factor in the ability of the carbocation to form and be stabilized. The CH···π interaction between the methyl groups of the *N*,*N*-dimethyl moiety of tabun and the side chains of Phe322, Trp298 of subunit A, and Phe51 of subunit C bring extra stability to the non-aged tabun complex. Finally, the binding of DFP, sarin, soman or tabun to gVIIA-PLA2 results in the placement of hydrophobic alkyl groups in positions that make the functionally significant active site atoms virtually inaccessible to water. The alkyl groups of the conjugates block an incoming water molecule and restrict any interaction with His351 as well. The exclusion of water from the active site in gVIIA-PLA2 complexes might be the key to understanding the lack of aged adducts. While it is known that for AChE and BChE, aging is an enzyme-catalyzed process, it is slow for most OP compounds compared to other enzyme-mediated processes. In light of the consensus mechanism for aging (Fig. 1), the current results are not surprising, since a carbocation must be formed by charge separation. Therefore, it would be reasonable to assume the change of dielectric of the surroundings would be a factor in the ability to form the carbocation. The more solvent accessible active sites of chymotrypsin, AChE and BChE yield a higher dielectric in their active sites, thus enabling these active sites to be reactivated by the attack of activated nucleophiles on their OP adducts. In contrast, gVIIA-PLA2 branched OP complexes are positioned with the alkyl chain blocking solvent access, and as a result lowering the local dielectrics surrounding key active site atoms.

In the present work, gVIIA-PLA2 has been identified as an additional enzyme that forms stable non-aged complexes of nerve agents, such as DFP, sarin, soman and tabun. The enzymes carboxylesterase and gVIII-PLA2 are two other systems that have been shown to be resistant to aging, but each displays greater stereoselectivity for the nerve agents than does gVIIA-PLA2. Human carboxylesterase was shown to react preferentially with the less toxic P_R stereoisomer of soman and the P_S stereoisomer of tabun [18]. AChE reacts preferentially with the P_S stereoisomer of soman [34], and the P_R stereoisomers of tabun [35]. The gVIII-PLA2 enzyme was previously shown to react with the more toxic P_S stereoisomers of sarin and soman [19]. In the gVIII-PLA2 system, a crystal structure and GC/MS analysis of the sarin reaction gave convincing evidence of stereoselective preference of reaction [19]. This contrasts our present work, where we have shown that gVIIA-PLA2 reacts non-selectively with both P_R and P_S stereoisomers of sarin and soman. In contrast, the enzyme showed stereospecificity for the more toxic P_R stereoisomer of tabun. Together, the nascent reactivity of gVIIA-PLA2 with sarin, soman and tabun serves as a starting point to engineer the enzyme to display OP hydrolase activity, which has already enjoyed limited success in other serine hydrolases [36,37]. This approach contrasts with other catalytic bioscavengers in development that utilize a mechanism in which the initial attack is by a catalytic water molecule [38]. However, despite notable catalytic efficiencies, these enzymes typically have high K_M values; therefore they suffer from an inability to efficiently bind OP compounds at concentrations shown to be lethal in test animals. The structural characterization of the interactions between the oxyanion hole of gVIIA-PLA2 and the OP adducts of DFP, sarin, soman and tabun may allow the rational development of a catalytic hydrolase with a lower K_M value than enzymes like paraoxonase [38] or phosphotriesterase [39]. The versatility of the gVIIA-PLA2 active site is currently being exploited to generate, through mutagenesis, catalytic bioscavengers of highly toxic OPs that will work at the physiologically relevant and low concentrations of OPs that are known or estimated to be toxic *in vivo*.

Acknowledgements

We thank ICOS Corp. for supplying us with the protein PAFase. We thank Dr. James Dillman and Ms. Lisa Bottalico for obtaining MALDI-MS data and Mr. Rick Smith for helping to complete the GC/MS analysis at the USAMRICD. We also thank the support staff of 19ID and 24ID beam lines of Advance Photon Source at the Argonne National Laboratory for assistance during X-ray diffraction data collection.

Appendix A. Supplementary data

Supplementary data associated with this article can be found, in the online version, at doi:10.1016/j.bcp.2009.04.018.

References

[1] Schaloske RH, Dennis EA. The phospholipase A2 superfamily and its group numbering system. Biochim Biophys Acta 2006;1761:1246–59.
[2] Tjoelker LW, Eberhardt C, Unger J, Trong HL, Zimmerman GA, McIntyre TM, et al. Plasma platelet-activating factor acetylhydrolase is a secreted phospholipase A2 with a catalytic triad. J Biol Chem 1995;270:25481–7.
[3] Stremler KE, Stafforini DM, Prescott SM, McIntyre TM. Human plasma platelet-activating factor acetylhydrolase. Oxidatively fragmented phospholipids as substrates. J Biol Chem 1991;266:11095–103.

[4] Davis B, Koster G, Douet LJ, Scigelova M, Woffendin G, Ward JM, et al. Electrospray ionization mass spectrometry identifies substrates and products of lipoprotein-associated phospholipase A(2) in oxidized human low density lipoprotein. J Biol Chem 2008;283:6428–37.
[5] Macphee CH, Nelson JJ. An evolving story of lipoprotein-associated phospholipase A2 in atherosclerosis and cardiovascular risk prediction. Eur Heart J 2005;26:107–9.
[6] Min JH, Jain MK, Wilder C, Paul L, Apitz-Castro R, Aspleaf DC, et al. Membrane-bound plasma platelet activating factor acetylhydrolase acts on substrate in the aqueous phase. Biochemistry 1999;38:12935–42.
[7] Min JH, Wilder C, Aoki J, Arai H, Inoue K, Paul L, et al. Platelet-activating factor acetylhydrolases: broad substrate specificity and lipoprotein binding does not modulate the catalytic properties of the plasma enzyme. Biochemistry 2001;40:4539–49.
[8] Samanta U, Bahnson BJ. Crystal structure of human plasma platelet-activating factor acetylhydrolase: structural implication to lipoprotein binding and catalysis. J Biol Chem 2008;283:31617–24.
[9] Casida JE, Quistad GB. Organophosphate toxicology: safety aspects of nonacetylcholinesterase secondary targets. Chem Res Toxicol 2004;17: 983–98.
[10] Millard CB, Kryger G, Ordentlich A, Greenblatt HM, Harel M, Raves ML, et al. Crystal structures of aged phosphonylated acetylcholinesterase: nerve agent reaction products at the atomic level. Biochemistry 1999;38:7032–9.
[11] Michel HO, Hackley BE, Berkowitz L, List G, Hackley EB, Gilliam W, et al. Ageing and dealkylation of soman (pinacolylmethylphosphonofluoridate)-inactivated eel cholinesterase. Arch Biochem Biophys 1967;121:29–34.
[12] Harris LW, Fleisher JH, Clark J, Cliff WF. Dealkylation and loss of capacity for reactivation of cholinesterase inhibited by sarin. Science 1966;154:404–7.
[13] Broomfield CA, Lockridge O, Millard CB. Protein engineering of a human enzyme that hydrolyzes V and G nerve agents: design, construction and characterization. Chem Biol Interact 1999;119–20:413–8.
[14] Hornberg A, Tunemalm AK, Ekstrom F. Crystal structures of acetylcholinesterase in complex with organophosphorus compounds suggest that the acyl pocket modulates the aging reaction by precluding the formation of the trigonal bipyramidal transition state. Biochemistry 2007;46:4815–25.
[15] Millard CB, Koellner G, Ordentlich A, Shafferman A, Silman I, Sussman JL. Reaction products of acetylcholinesterase and VX reveal a mobile histidine in the catalytic triad. J Am Chem Soc 1999;121:9883–4.
[16] Nachon F, Asojo OA, Borgstahl GEO, Masson P, Lockridge O. Role of water in aging of human butyrylcholinesterase inhibited by echothiophate: the crystal structure suggests two alternative mechanisms of aging. Biochemistry 2005;44:1154–62.
[17] Carletti E, Li H, Li B, Ekstrom F, Nicolet Y, Loiodice M, et al. Aging of cholinesterases phosphylated by tabun proceeds through *O*-dealkylation. J Am Chem Soc 2008;130:16011–20.
[18] Fleming CD, Edwards CC, Kirby SD, Maxwell DM, Potter PM, Cerasoli DM, et al. Crystal structures of human carboxylesterase 1 in covalent complexes with the chemical warfare agents soman and tabun. Biochemistry 2007;46:5063–71.
[19] Epstein TM, Samanta U, Kirby SD, Cerasoli DM, Bahnson BJ. Crystal structures of brain group-VIII phospholipase A2 in nonaged complexes with the organophosphorus nerve agents soman and sarin. Biochemistry 2009;48:3425–35.
[20] Samanta U, Wilder C, Bahnson BJ. Crystallization and preliminary X-ray crystallographic analysis of human plasma platelet activating factor acetylhydrolase. Protein Pept Lett 2009;16:97–100.
[21] Otwinowski Z, Minor W. Processing of X-ray diffraction data collected in oscillation mode. Meth Enzymol 1997;276:307–26.
[22] CCP4. The CCP4 Suite: programs for protein crystallography. Acta Crystallogr D: Biol Crystallogr 1994;50:760–3.
[23] Emsley P, Cowtan K. Coot: model-building tools for molecular graphics. Acta Crystallogr D Biol Crystallogr 2004;60:2126–32.
[24] Murshudov GN, Vagin AA, Dodson EJ. Refinement of macromolecular structures by the maximum-likelihood method. Acta Crystallogr D Biol Crystallogr 1997;53:240–55.
[25] Masson P, Fortier PL, Albaret C, Froment MT, Bartels CF, Lockridge O. Aging of di-isopropyl-phosphorylated human butyrylcholinesterase. Biochem J 1997;327:601–7.
[26] Yeung DT, Smith JR, Sweeney RE, Lenz DE, Cerasoli DM. Direct detection of stereospecific soman hydrolysis by wild-type human serum paraoxonase. FEBS J 2007;274:1183–91.
[27] Chakrabarti P, Samanta U. CH/pi interaction in the packing of the adenine ring in protein structures. J Mol Biol 1995;251:9–14.
[28] Samanta U, Chakrabarti P, Chandrasekhar J. Ab initio study of energetics of X–H center dot center dot center dot pi (X = N, O, and C) interactions involving a heteroaromatic ring. J Phys Chem A 1998;102:8964–9.
[29] Nishio M, Hirota M, Umezawa Y. The CH/pi interaction: nature, evidence and consequences. New York: Wiley-VCH; 1998.
[30] Kossiakoff AA. Basic Life Sci 1984;27:281–304.
[31] Millard CB, Kryger G, Ordentlich A, Greenblatt HM, Harel M, Raves ML, et al. Biochemistry 1999;38:7032–9.
[32] Ordentlich A, Barak D, Kronman C, Benschop HP, De Jong LP, Ariel N, et al. Exploring the active center of human acetylcholinesterase with stereomers of an organophosphorus inhibitor with two chiral centers. Biochemistry 1999;38: 3055–66.
[33] Barak D, Ordentlich A, Segall Y, Velan B, Benschop HP, De Jong LPA, et al. Carbocation-mediated processes in biocatalysts. Contribution of aromatic moieties. J Am Chem Soc 1997;119:3157–8.
[34] Benschop HP, Konings CA, Van Genderen J, De Jong LP. Isolation, anticholinesterase properties, and acute toxicity in mice of the four stereoisomers of the nerve agent soman. Toxicol Appl Pharmacol 1984;72:61–74.
[35] Ekstrom F, Pang YP, Boman M, Artursson E, Akfur C, Borjegren S. Crystal structures of acetylcholinesterase in complex with HI-6, Ortho-7 and obidoxime: structural basis for differences in the ability to reactivate tabun conjugates. Biochem Pharmacol 2006;72:597–607.
[36] Lockridge O, Blong RM, Masson P, Froment MT, Millard CB, Broomfield CA. A single amino acid substitution, Gly117His, confers phosphotriesterase (organophosphorus acid anhydride hydrolase) activity on human butyrylcholinesterase. Biochemistry 1997;36:786–95.
[37] Millard CB, Lockridge O, Broomfield CA. Organophosphorus acid anhydride hydrolase activity in human butyrylcholinesterase: synergy results in a somanase. Biochemistry 1998;37:237–47.
[38] Amitai G, Gaidukov L, Adani R, Yishay S, Yacov G, Kushnir M, et al. Enhanced stereoselective hydrolysis of toxic organophosphates by directly evolved variants of mammalian serum paraoxonase. FEBS J 2006;273:1906–19.
[39] Ghanem E, Raushel FM. Detoxification of organophosphate nerve agents by bacterial phosphotriesterase. Toxicol Appl Pharmacol 2005;207:459–70.
[40] Brunger AT. The free *R* value: a novel statistical quantity for assessing the accuracy of crystal structures. Nature 1992;355:472–4.
[41] DeLano WL. The PyMOL user's manual. Palo Alto, CA, USA: DeLano Scientific; 2002.